

## Article

# Optimal Design of the Shape of a Non-Ball Mandrel for Thin-Walled Tube Small Radius Cold Bending

Lu Bai <sup>1,2,3</sup>, Jun Liu <sup>1,2,3,\*</sup>, Ziang Wang <sup>1,2,3</sup> and Shuanggui Zou <sup>4</sup>

<sup>1</sup> State Key Laboratory of Ocean Engineering, Shanghai Jiao Tong University, Shanghai 200240, China; bailu0918@sjtu.edu.cn (L.B.); vt0275@alumni.sjtu.edu.cn (Z.W.)

<sup>2</sup> Collaborative Innovation Center for Advanced Ship and Deep-Sea Exploration, Shanghai Jiao Tong University, Shanghai 200240, China

<sup>3</sup> Department of Naval Architecture and Ocean Engineering, Shanghai Jiao Tong University, Shanghai 200240, China

<sup>4</sup> CSSC Guangzhou Longxue Pipe System Co., Ltd., Guangzhou 511462, China; zousg@chinagsi.com

\* Correspondence: jliu@sjtu.edu.cn

**Abstract:** In the field of cold bending, it is necessary to use ball mandrels, especially to bend thin-walled tubes with a small radius. However, the bending process with a ball mandrel is complex and expensive, and it is easy to jam the core ball inside the tube. To solve these issues, we designed two kinds of hollow non-ball mandrel schemes with low stiffness that were suitable for the small radius bending of thin-walled tubes. We evaluated the forming quality of cold bending numerically and the influence of the hollow section length and thickness on the forming indices. Our results showed that the thickness of the hollow section has a greater influence on forming quality than the length. As the hollow section's thickness increased, the wrinkling rate first declined by approximately 40% and then increased by above 50%. When the thickness was 11 mm in scheme 1 and 13 mm in scheme 2, the wrinkling rate reached minimum values of 1.32% and 1.50%, respectively. As the hollow section's thickness increased, the flattening rate decreased by more than 60% and the thinning rate increased by about 40%. A multi-objective optimization of forming indices was carried out by ideal point method and grey wolf optimizer. By comparing the forming results before and after optimization, the feasibility of using the proposed hollow mandrel was proved, and the hollow mandrel scheme of standard cylinder is therefore recommended.



**Citation:** Bai, L.; Liu, J.; Wang, Z.; Zou, S. Optimal Design of the Shape of a Non-Ball Mandrel for Thin-Walled Tube Small Radius Cold Bending. *Metals* **2021**, *11*, 1221. <https://doi.org/10.3390/met11081221>

Academic Editors: Bin Liu, Kun Liu and Bernd-Arno Behrens

Received: 6 July 2021

Accepted: 28 July 2021

Published: 30 July 2021

**Publisher's Note:** MDPI stays neutral with regard to jurisdictional claims in published maps and institutional affiliations.



**Copyright:** © 2021 by the authors. Licensee MDPI, Basel, Switzerland. This article is an open access article distributed under the terms and conditions of the Creative Commons Attribution (CC BY) license (<https://creativecommons.org/licenses/by/4.0/>).

**Keywords:** hollow mandrel; thin-walled tube; cold bending; multi-objective optimization

## 1. Introduction

In manufacturing fields, such as aerospace, automotive engineering, and marine and ocean engineering, tubes bent with a relative wall thickness ( $t/D$ ) of less than 5% and relative bending radius ( $R/D$ ) of less than 2 are often used to meet lightweight, high-strength, and space-saving requirements [1]. The forming quality of thin-walled tubes is influenced by many factors including the material used, geometric characteristics of tubes, and process parameters of molds, among others. The design of the mandrel is of great importance and plays a key role in improving the forming quality of the tube.

In previous research of mandrel design, experimental methods have been widely used. Given the widespread use of numerical simulations, these methods, along with experimental verification, are most often used to study the influence of different factors on the small radius bending of thin-walled tubes. Through numerical and experimental methods, Liu et al. found that the tube material, number of core balls, and extension length of the mandrel significantly influence the bending forming quality of thin-walled steel tubes for automotive bumpers [2]. Shen et al. discussed the influence of mandrel parameters on forming quality based on experimental results [3]. Nakajima et al. fabricated an aluminum alloy rectangular tube and analyzed the pear-shaped deformation peculiar

to the ultra-thin wall tube by means of finite element method [4]. Utsumi et al. proposed a laminated elastic mandrel consisting of nylon and PVC plates and studied the influence of certain parameters on the forming quality using numerical and experimental methods [5].

Optimization based on experimental and numerical results is an important element of engineering. Optimization methods have been widely studied in recent years. Using the topology optimization based on the finite element method, Różyło decreased the I-section profile's volume by 25% [6]. Tsumura proposed a hierarchically distributed optimization algorithm which decreased the amount of data transmission [7]. Chen et al. proposed a multiplexed optimization method with a significantly reduced computation load [8]. Farzampour et al. used the grey wolf optimizer to maximize the energy dissipation capacity and reduce the plastic strain concentration [9]. Meanwhile, many new optimization algorithms have been applied in the study of mandrel design. The stress and strain state and forming quality of thin-walled aluminum tubes have been studied under different relative bending radius, which led to an algorithm being proposed to improve the forming quality of tube bending [10–12]. Zhao et al. established a genetic algorithm model with mandrel parameters as variables to predict the forming results of different small radius tubes [13]. Wang et al. optimized the shape parameters of the mandrel head based on the orthogonal experimental design method [14].

Here, we focus on the mandrel shape as a means to improve the forming quality of thin-walled tubes. The mandrel can be categorized as either a ball mandrel or non-ball mandrel according to whether the core ball is used or not. When the thin-walled tube is bent with a small radius, the ideal forming result cannot be obtained because of the excessive stiffness of the non-ball mandrel, so the ball mandrel shown in Figure 1 is often used for bending in engineering. In order to study the applicability of different kinds of mandrels, Dang proposed a method to determine whether to use a core ball according to relative bending radius, relative wall thickness, and bending angle [15]. Wu et al. compared the effects of a cylinder mandrel, round mandrel, arc mandrel, ball mandrel, and round ball mandrel on the forming quality and found that the ball mandrel gave the best outcome [16]. The core ball structure with low stiffness in the ball mandrel can provide support for thin-walled tubes and avoid the wrinkling deformation, so as to obtain sufficient forming quality. However, the core ball structure has many disadvantages that are seldom discussed. First, the process required is more complicated and expensive because the mandrels used in different tube bending systems have to be redesigned and processed. Furthermore, it is necessary to consider the connection between the core ball and core rod. In addition, the core ball can easily become jammed inside the tube while bending and cause wear on the inner side of the tube wall. Therefore, we attempted to design a non-ball mandrel with low stiffness to obtain a thin-walled bent tube that meets the quality requirements.

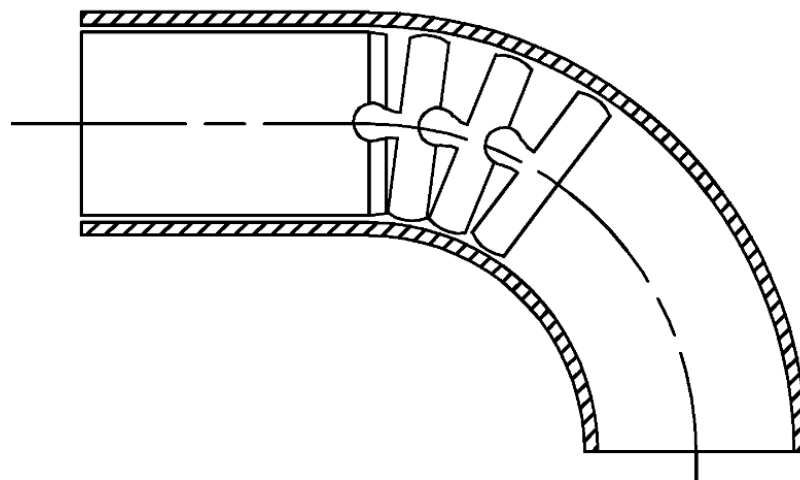


Figure 1. Ball mandrel.

In this paper, we consider two kinds of non-ball mandrel schemes with hollow sections and adopt a numerical method to simulate cold bending forming. Based on the numerical results, the influence of hollow section parameters on the bending forming indices is studied. The bending results of the two mandrel schemes are compared and the parameter optimization of the mandrel is realized by combining the multi-objective optimization method and grey wolf optimizer.

## 2. Materials and Methods

### 2.1. Modes of Behavior in Cold Bending

The stress state of the bent tube is shown in Figure 2. In the cold bending process, the outer side of the tube is elongated by tangential tension,  $\sigma_T$ , and the inner side is shortened by tangential pressure,  $\sigma_P$ . The tube is therefore thinned on the outer side of the bend and thickened on the inner side. The supporting forces  $N$  and  $N'$  are the result of tangential forces due to the flattening deformation of the transverse section.

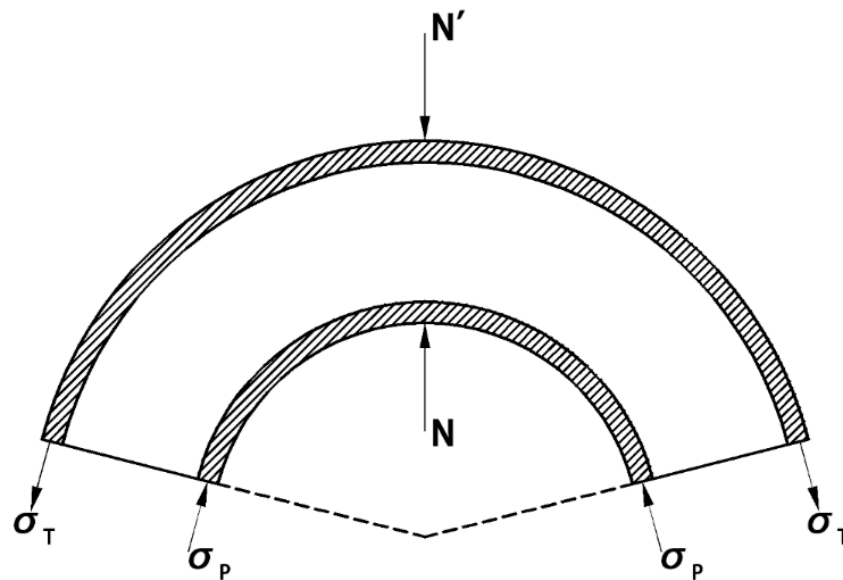


Figure 2. Stress state during cold bending.

The inner side of the tube can easily become wrinkled due to the circumferential and tangential pressure. As the pressure increases, local wrinkles may occur before the tube buckles. As the pressure continues to increase, buckling occurs at the inner side of the tube, and then an overall buckling wrinkle may occur. If the pressure exceeds the upper limit, over flattening may occur.

### 2.2. Numerical Method and Reliability Verification

We used a numerical simulation for this research. First, the cold bending process of steel tube with  $D = \phi 114$  mm and  $t = 8$  mm was simulated, and the validity of the analysis method was verified through a comparison with experimental results. Finite element models of the tube, arc mandrel, and bending molds were then established, as shown in Figure 3.

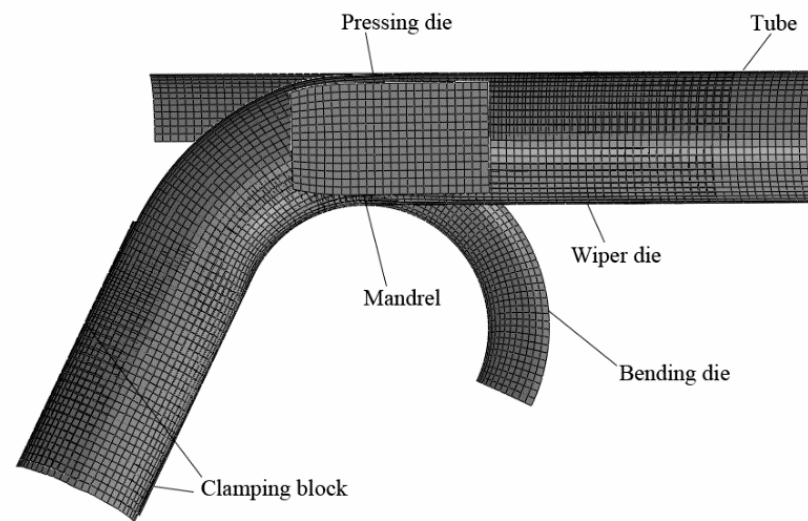


Figure 3. Finite element model.

The tube was made of No. 20 carbon steel and the mandrel was made of T235 steel. The bilinear isotropic constitutive relationship was used to model the material properties of tube and mandrel [17]. The stress–strain curve is shown in Figure 4. According to CCS Rules for Materials and Welding, the material parameters were determined as shown in Table 1.

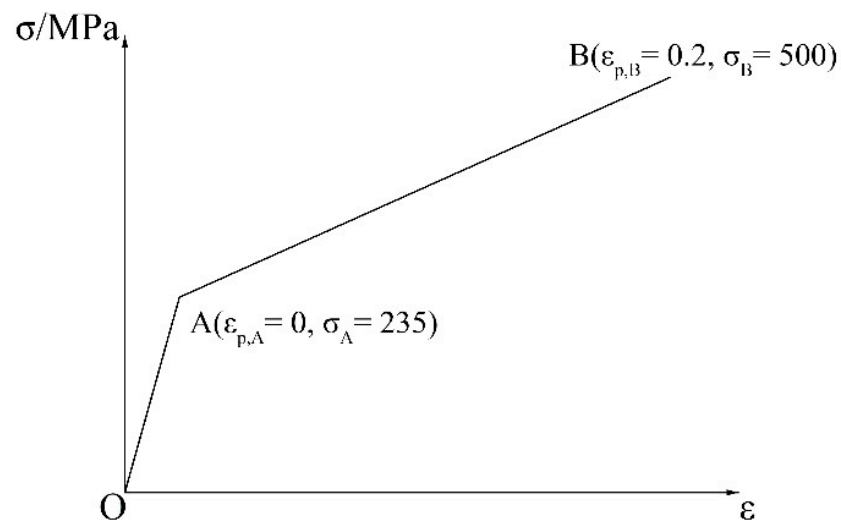


Figure 4. Stress–strain curve of the material. OA and AB represent the elastic and plastic stages, respectively,  $\sigma_A$  and  $\sigma_B$  represent the stress at points A and B, respectively,  $\sigma_A$  is the yield stress, and  $\varepsilon_{p,A}$  and  $\varepsilon_{p,B}$  represent the plastic strain at the two points.

Table 1. Material parameters.

$\rho^1/\text{kg}\times\text{m}^{-3}$	$E^2/\text{MPa}$	$\nu^3$	$\sigma_A/\text{MPa}$	$\varepsilon_{p,A}$	$\sigma_B/\text{MPa}$	$\varepsilon_{p,B}$
$7.84 \times 10^3$	206,000	0.3	235	0	500	0.2

<sup>1</sup>  $\rho$  is the density. <sup>2</sup>  $E$  is the elastic modulus. <sup>3</sup>  $\nu$  is the Poisson's ratio.

Considering the calculation accuracy and efficiency, the tube and mandrel were simulated by elastic-plastic properties, and all molds except the mandrel were simulated by a rigid body element. Mesh size selection has been studied in previous studies, which found similar results using a mesh size 1 and 0.75 times the tube wall thickness [18]. When the

mesh size was 1.5 times the tube wall thickness, it was too large to accurately describe the inner wrinkle, meaning the wrinkle height was not accurate [18]. When the mesh size was reduced to 0.75 times the tube wall thickness, the analysis time was excessive, while using a mesh size smaller than the plate thickness is not recommended [18,19]. Therefore, the mesh size used was the same as the tube wall thickness.

Constraint conditions were determined according to the actual bending process. During the bending process, the mandrel and the wiper die remain motionless, restricting their degrees of freedom in all directions. The clamping block and the bending die rotate around the center of the bending path, so they were set to the corresponding angular velocity. The pressing die applies pressure to the outer wall of the tube during bending, so it was considered to move in a straight line with a certain linear speed.

Tube bending mainly depends on the contact between the tube and the mold. In order to ensure that the tube nodes cannot penetrate the surface of the mold, the dynamic constraint method was used to define the contact between the tube and the clamping block, bending die, pressing die, wiper die, and mandrel. The friction generated by contact was simulated by means of Coulomb friction. The friction coefficient of the contact surface is shown in Table 2.

**Table 2.** Coefficient of friction.

Contact Surface	Tube-Clamping Block	Tube-Bending Die	Tube-Pressing Die	Tube-Wiper Die	Tube-Mandrel
Friction coefficient	No relative slip	0.15	0.15	0.10	0.05

To verify the numerical simulation method, a steel tube with  $D = \phi 114$  mm and  $t = 8$  mm was tested. The mandrel parameters used in the experiment are listed in Table 3. A  $90^\circ$  bending experiment was carried out on the target steel tube. The experimental and numerical results of the bending are shown in Table 4. The distribution of wall thickness and wrinkle height of the bent tube are shown in Figure 5. The wrinkle height in the numerical simulation was 2.106 mm, while the wrinkle in the experiment was difficult to measure. The error of wrinkle is within the acceptable range and the minimum wall thickness was similar, indicating that the simulation method was reliable.

**Table 3.** Test parameter settings.

Clearance between Mandrel and Tube/mm	Radius of Curvature at the Mandrel Head/mm	Curve Segment Length of Mandrel/mm	Mandrel Extension/mm
1	220	50	12

**Table 4.** Experimental and numerical results of bending.

	Experimental Result	Numerical Result	Error
Minimum wall thickness/mm	6.3	6.351	0.81%
Wrinkle	No obvious wrinkle was measured	The maximum wrinkle height was 2.106 mm	<2% of tube diameter

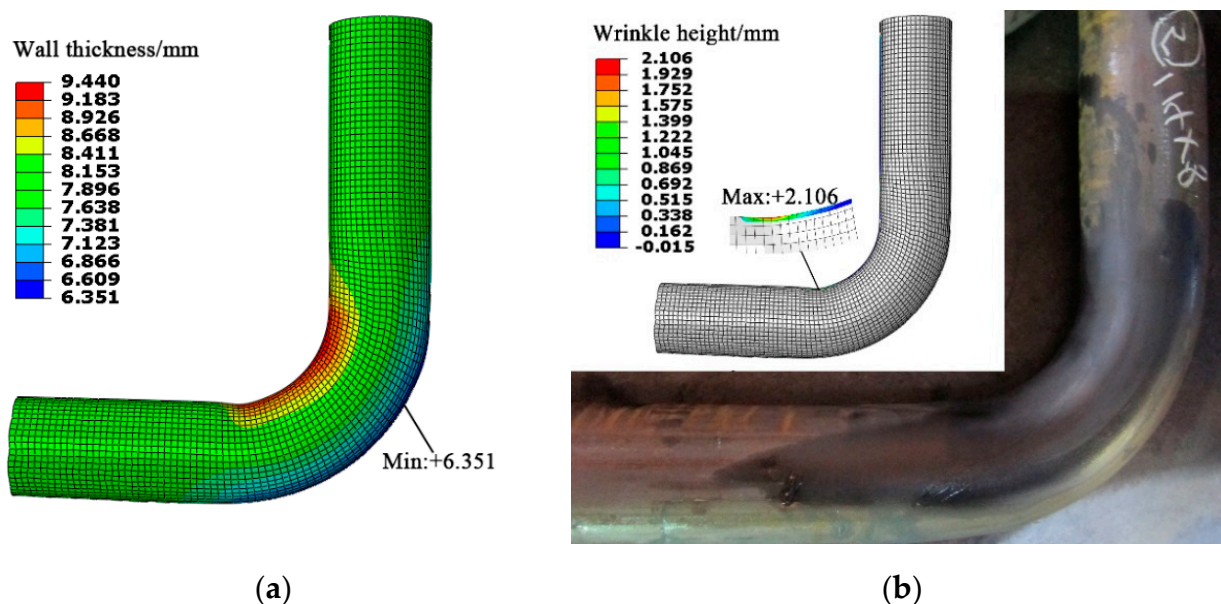


**Figure 5.** The distribution of wall thickness and wrinkle height of the bent tube: (a) the distribution of wall thickness and (b) the distribution of wrinkle height.

### 2.3. Hollow Mandrel Shape Design for Thin-Walled Tube Bending

Taking the tube with  $D = \phi 95$  mm and  $t = 4.5$  mm as an example, the cold bending numerical simulation was performed using the ordinary non-ball arc mandrel. To evaluate the quality of tube bending, three indices of wrinkling rate,  $I_w$ , flattening rate,  $I_f$ , and thinning rate,  $I_t$ , are defined by Equations (1)–(3). According to the GB/T 34000-2016 China Shipbuilding Quality Standard,  $I_w$ ,  $I_f$  and  $I_t$  of cold bending tube should not exceed 2%, 10%, and 25%, respectively.

$$I_w = H_w / D_0 \quad (1)$$

$$I_f = (D_0 - D') / D_0 \quad (2)$$

$$I_t = (t_0 - t') / t_0 \quad (3)$$

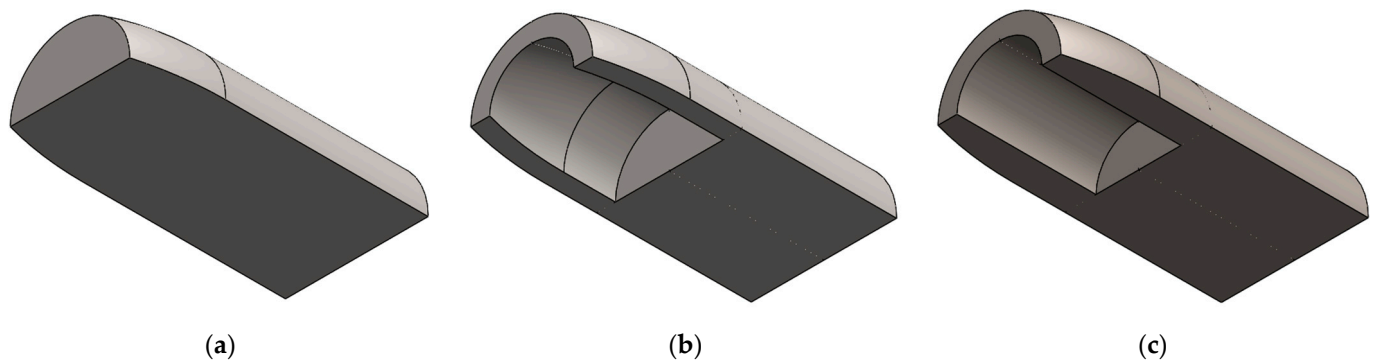
where  $H_w$  is the maximum wrinkle height of the tube,  $D_0$  is the initial diameter of the tube,  $D'$  is the minimum diameter of the tube section after bending,  $t_0$  is the initial wall thickness of the tube, and  $t'$  is the wall thickness at the thinnest part of the tube after bending.

Table 5 shows the calculated values of forming indices of the tube with  $D = \phi 95$  mm and  $t = 4.5$  mm; it can be seen that the wrinkling rate did not meet the quality requirement due to the excessive stiffness of the mandrel head.

**Table 5.** Forming results of the thin-walled tube using an ordinary non-ball mandrel.

$I_w/\%$	$I_f/\%$	$I_t/\%$
2.44	8.94	19.92

To reduce the stiffness of the mandrel and improve the forming quality, the hollow mandrel schemes shown in Figure 6b,c were designed for thin-walled tubes on the basis of the ordinary non-ball mandrel (Figure 6a). The mandrel shown in Figure 6b was defined as hollow mandrel scheme 1 and the mandrel shown in Figure 6c was defined as hollow mandrel scheme 2.



**Figure 6.** Different types of mandrel: (a) ordinary non-ball mandrel, (b) hollow mandrel scheme 1, and (c) hollow mandrel scheme 2.

The two hollow mandrel schemes we proposed and the shape of hollow section can be defined by the length,  $L$ , and thickness,  $t$ , as shown in Figure 7. In scheme 1 (shown in Figure 7a), a section of cylinder-like body was cut off, and the surface of the inner wall and outer wall were parallel; therefore, the thickness of the hollow section remained unchanged. In scheme 2 (shown in Figure 7b), a regular cylinder was cut off and the inner wall was a regular cylinder, so the thickness of the hollow section varied.

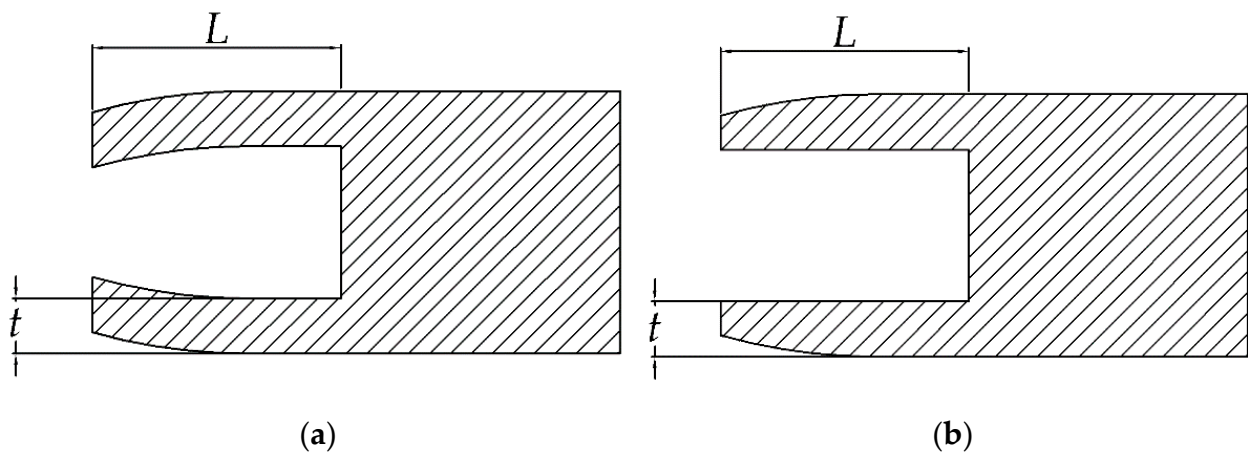


**Figure 7.** The shape of the hollow mandrel section in (a) hollow mandrel scheme 1 and (b) hollow mandrel scheme 2.

### 3. Results and Discussion

#### 3.1. Simulation Results and Analysis of Hollow Mandrel

To obtain a suitable hollow mandrel for the tube with  $D = \phi 95$  mm and  $t = 4.5$  mm, various hollow mandrel parameter cases were designed (Tables 6 and 7) and cold bending using the mandrels with different section sizes was simulated. The forming simulation was performed with a bending angle of  $90^\circ$  and a bending radius of 137 mm. According to experience from trial calculations, for scheme 1 five hollow section lengths were selected (60, 80, 100, 120 and 140 mm) and nine hollow section thicknesses were selected (6, 7, 8, 9, 10, 11, 12, 15 and 20 mm). For scheme 2, the selection of hollow section lengths was the same and nine hollow section thicknesses were selected (8, 9, 10, 11, 12, 13, 14, 15 and 20 mm). Ninety bending simulations were performed for the two hollow mandrel schemes. The calculated forming results are listed in Tables 6 and 7, and the stress distribution of the 33rd simulation result of section schemes 1 and 2 is shown in Figures 8 and 9.

**Table 6.** Hollow mandrel scheme 1 forming results.

No.	L/mm	t/mm	$I_w/\%$	$I_f/\%$	$I_t/\%$	No.	L/mm	t/mm	$I_w/\%$	$I_f/\%$	$I_t/\%$
1	60	6	2.47	17.86	13.69	24	100	11	1.36	8.15	19.25
2	60	7	2.25	11.48	15.09	25	100	12	1.60	7.53	19.29
3	60	8	1.98	10.02	17.37	26	100	15	2.44	8.78	19.76
4	60	9	2.13	9.86	18.59	27	100	20	2.51	8.88	19.54
5	60	10	1.92	8.39	19.01	28	120	6	2.52	23.44	13.01
6	60	11	1.54	8.28	19.62	29	120	7	2.23	15.90	14.84
7	60	12	2.42	9.94	19.56	30	120	8	1.88	13.01	16.46
8	60	15	2.49	8.88	19.98	31	120	9	1.97	10.66	17.76
9	60	20	2.51	8.95	19.64	32	120	10	1.76	8.87	18.55
10	80	6	2.55	22.81	13.29	33	120	11	1.32	8.11	19.24
11	80	7	2.41	15.15	15.03	34	120	12	1.56	7.63	19.12
12	80	8	1.84	11.85	16.61	35	120	15	2.49	9.87	19.19
13	80	9	2.00	10.67	17.92	36	120	20	2.51	9.07	19.49
14	80	10	1.85	8.24	18.61	37	140	6	2.44	24.33	13.00
15	80	11	1.38	7.90	19.45	38	140	7	2.17	16.14	14.67
16	80	12	1.60	7.78	19.34	39	140	8	1.87	12.88	16.50
17	80	15	2.52	9.25	19.80	40	140	9	1.98	10.86	17.64
18	80	20	2.55	9.00	19.55	41	140	10	1.83	9.04	18.43
19	100	6	2.99	23.74	13.13	42	140	11	1.41	8.23	19.30
20	100	7	2.08	15.28	14.96	43	140	12	1.61	7.89	19.15
21	100	8	1.90	12.63	16.50	44	140	15	2.52	9.18	19.50
22	100	9	1.95	10.59	17.64	45	140	20	2.43	10.05	19.29
23	100	10	1.87	9.36	18.45						

**Table 7.** Hollow mandrel scheme 2 forming results.

No.	L/mm	t/mm	$I_w/\%$	$I_f/\%$	$I_t/\%$	No.	L/mm	t/mm	$I_w/\%$	$I_f/\%$	$I_t/\%$
1	60	8	1.78	21.08	13.57	24	100	13	1.62	8.86	19.14
2	60	9	2.11	19.02	15.57	25	100	14	2.42	9.66	19.22
3	60	10	2.03	11.26	17.77	26	100	15	2.46	9.39	19.04
4	60	11	1.91	10.23	19.03	27	100	20	2.52	8.68	19.89
5	60	12	1.65	9.02	18.73	28	120	8	2.51	27.22	12.71
6	60	13	2.28	9.63	19.19	29	120	9	2.18	23.58	14.55
7	60	14	2.44	9.23	19.10	30	120	10	1.96	15.03	16.42
8	60	15	2.60	9.43	19.12	31	120	11	1.80	10.52	17.83
9	60	20	2.41	9.24	19.84	32	120	12	1.47	9.72	18.40
10	80	8	2.69	27.02	12.67	33	120	13	1.50	8.26	19.13
11	80	9	2.15	22.50	14.59	34	120	14	2.46	9.81	19.27
12	80	10	2.04	13.33	16.29	35	120	15	2.54	9.30	19.00
13	80	11	1.84	10.68	17.98	36	120	20	2.30	8.35	19.79
14	80	12	1.51	8.75	18.54	37	140	8	2.55	27.26	12.76
15	80	13	1.59	8.47	18.85	38	140	9	2.17	24.30	14.50
16	80	14	2.35	9.81	19.18	39	140	10	1.90	14.03	16.56
17	80	15	2.55	9.41	19.05	40	140	11	1.84	10.62	18.08
18	80	20	2.44	8.91	19.74	41	140	12	1.53	9.43	18.64
19	100	8	2.52	27.23	12.77	42	140	13	1.51	8.41	18.98
20	100	9	2.15	24.04	14.52	43	140	14	2.45	9.52	19.03
21	100	10	1.94	14.66	16.50	44	140	15	2.44	9.39	18.86
22	100	11	1.90	10.96	18.00	45	140	20	2.45	8.77	19.90
23	100	12	1.47	9.63	18.49						

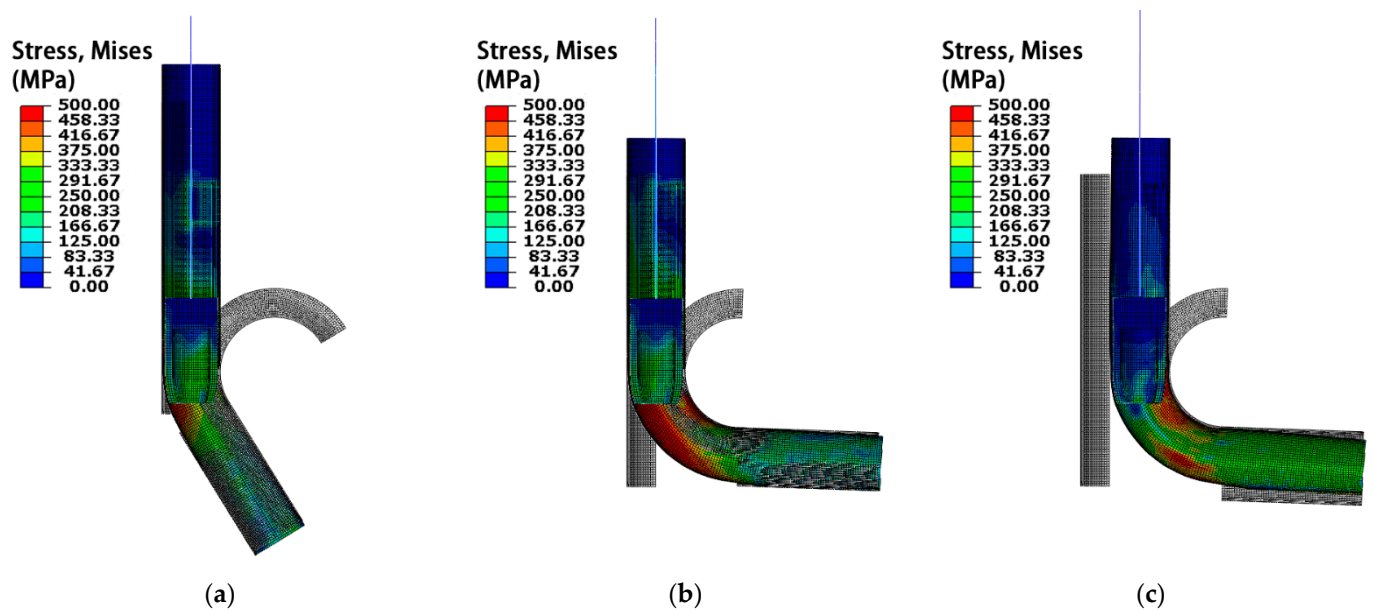


Figure 8. Stress distribution of hollow mandrel scheme 1: (a) bending step; (b) end of bending step; (c) unloading step.

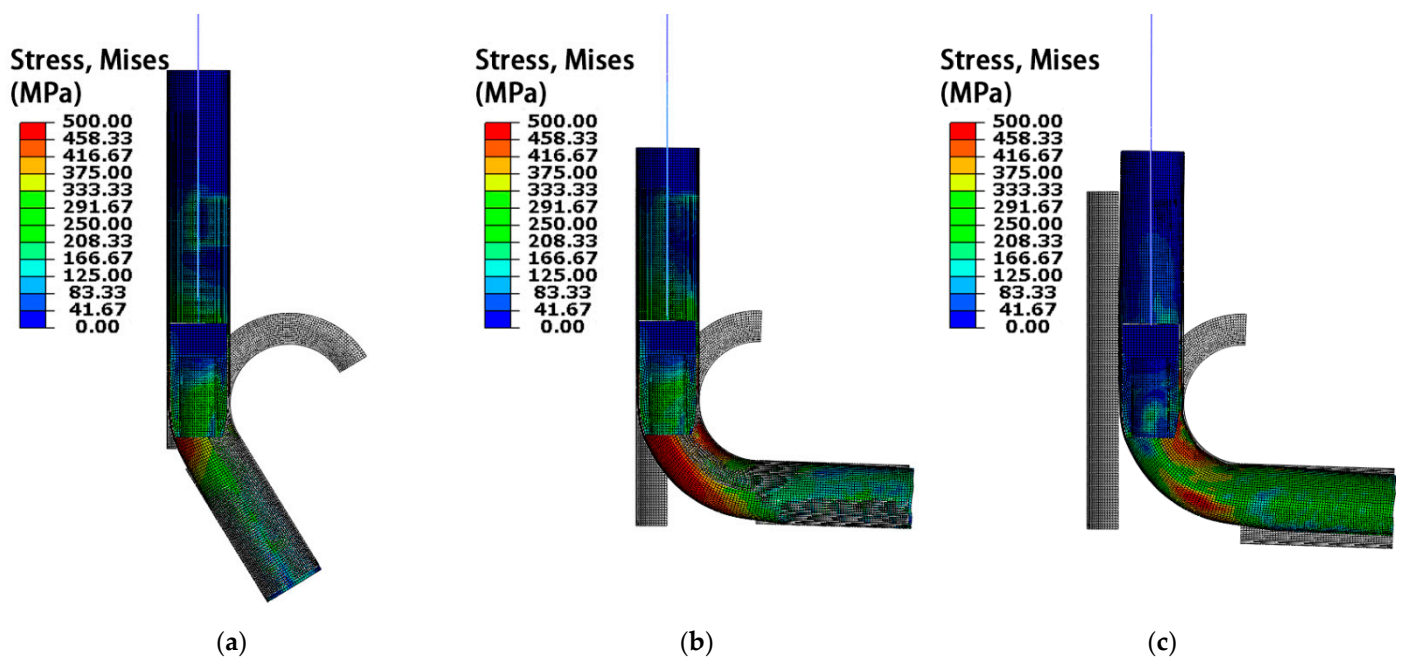


Figure 9. Stress distribution of hollow mandrel scheme 2: (a) bending step; (b) end of bending step; (c) unloading step.

Figure 10a,b shows the influence curves of hollow section parameters on the wrinkling rate,  $I_w$ . It can be seen that hollow section thickness,  $t$ , has a greater influence on  $I_w$  than the hollow section length,  $L$ . In scheme 1, as  $t$  increases from 6 to 11 mm, the mandrel stiffness gradually suits the bending of the thin-walled tube and  $I_w$  decreases significantly by 45.58%. When  $t$  is 11 mm,  $I_w$  reaches its minimum value. When  $t$  rises from 11 to 15 mm, the stiffness of the mandrel increases and it cannot provide sufficient support for the compression side of the tube, resulting in a 78.21% increase in  $I_w$ . The trend of influence on  $I_w$  in scheme 2 is basically the same as that in scheme 1. As  $t$  increases from 8 to 13 mm,  $I_w$  significantly reduces by 39.41% because the mandrel stiffness decreases to adapt to the tube wall thickness.  $I_w$  is lowest when  $t$  reaches 13 mm. When  $t$  rises from 13 to 15 mm,

$I_w$  increases by 51.44% because the stiffness of the mandrel becomes unsuitable for the thin-walled tube.

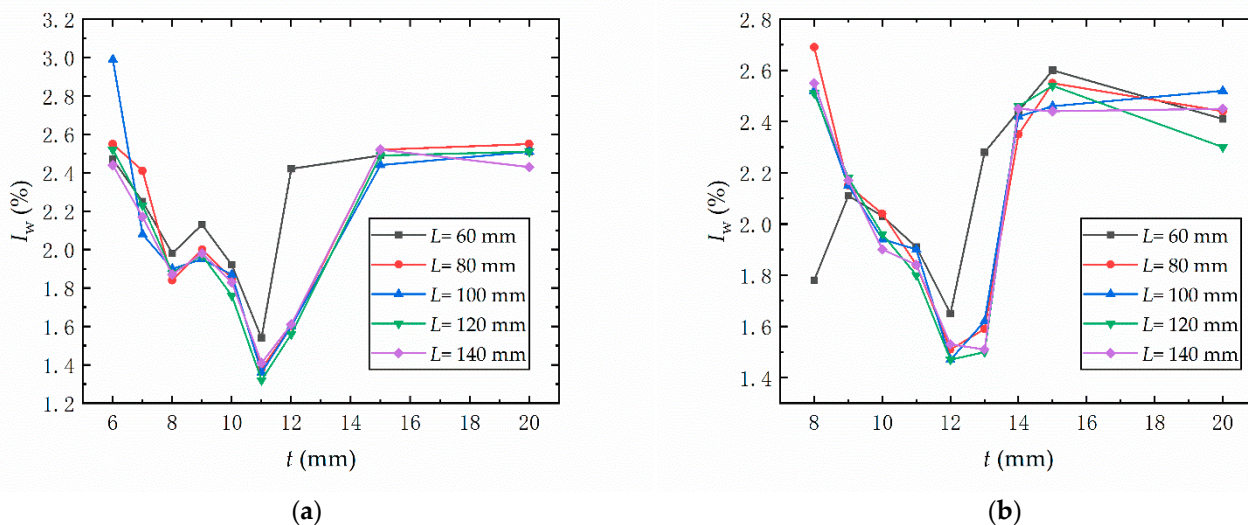


Figure 10. Influence of hollow section parameters on  $I_w$ : (a) hollow mandrel scheme 1; (b) hollow mandrel scheme 2.

Figure 11a,b shows the influence curves of hollow section parameters on the flattening rate,  $I_f$ . It can be seen that the trend of influence on  $I_f$  in the two schemes is essentially the same.  $I_f$  decreases with increasing  $t$  and decreasing  $L$ . In scheme 1, when  $t$  increases from 6 to 10 mm, the stiffness of the mandrel increases, providing more support for the inner side of the tube wall, so  $I_f$  decreases significantly by 60.49%. In scheme 2,  $I_f$  decreases by 63.83% when  $t$  increases from 8 to 12 mm. When the stiffness of the mandrel is increased to a certain extent, the influence of  $L$  and  $t$  on  $I_f$  begins to decrease, and  $I_f$  begins to fluctuate slightly. This is because, as the volume of the hollow section decreases, the supporting effect of the mandrel on the inner wall of the tube increases, which makes the tube's resistance to cross-section distortion stronger and leads to lower  $I_f$ .

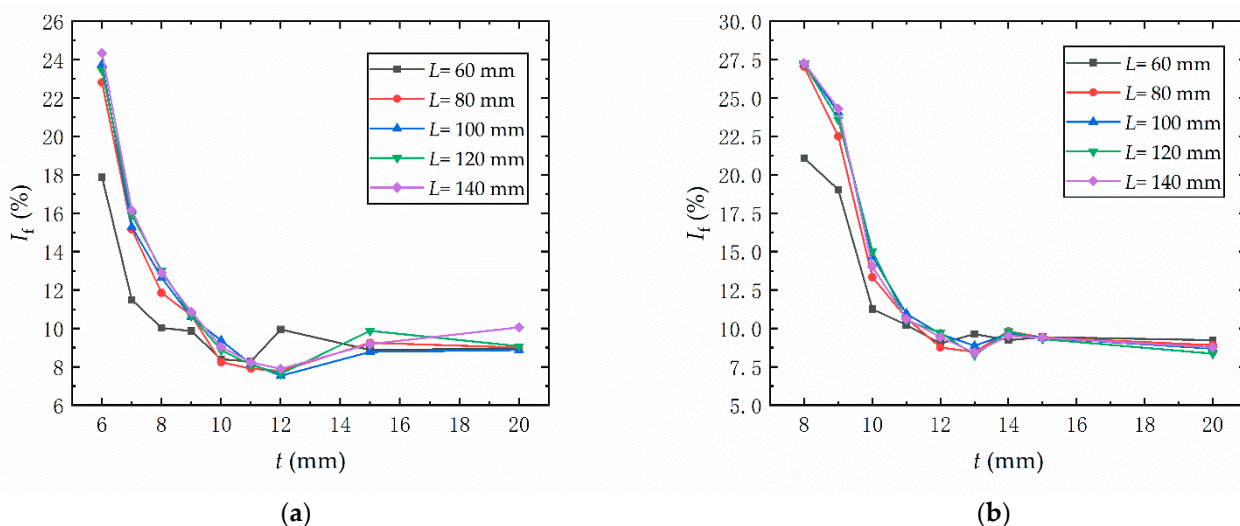


Figure 11. Influence of hollow section parameters on  $I_f$ : (a) hollow mandrel scheme 1; (b) hollow mandrel scheme 2.

Figure 12a,b shows the influence curves of hollow section parameters on the thinning rate  $I_t$ . It can be seen that the trend of influence on  $I_t$  in the two schemes is basically the same.  $I_t$  rises with increasing  $t$  and decreasing  $L$ . In scheme 1, when  $t$  increases from 6 to 9 mm, the stiffness of the hollow mandrel increases, which provides more support for the inner wall, and  $I_t$  increases significantly by 35.44%. In scheme 2,  $I_t$  increases by 41.02%

when  $t$  increases from 8 to 11 mm. When the stiffness of the mandrel is increased to a certain extent, the influence of  $L$  and  $t$  begins to decrease and  $I_t$  fluctuates and increases slightly. In general,  $I_t$  increases with increasing  $t$  and decreasing  $L$ . This is as the volume of the hollow section decreases, the friction of the mandrel on the inner wall of the tube increases, which strengthens the tube's thinning and leads to an increased  $I_t$ .

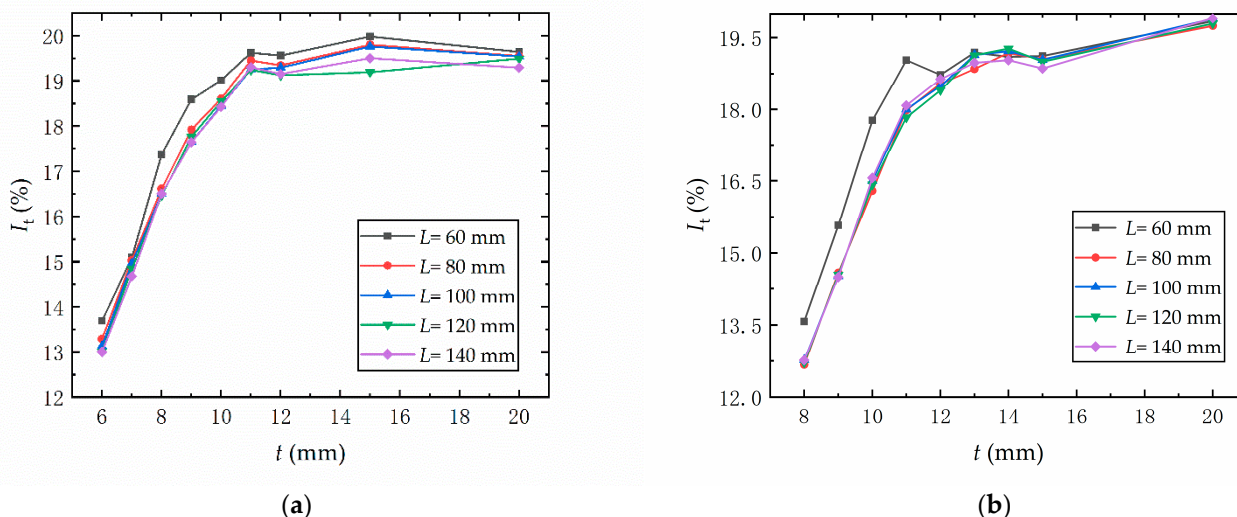


Figure 12. Influence of hollow section parameters on  $I_t$ : (a) hollow mandrel scheme 1; (b) hollow mandrel scheme 2.

### 3.2. Multi-Objective Optimization of Hollow Mandrel Parameters

The forming quality of the bent tube is determined by  $I_w$ ,  $I_f$  and  $I_t$ . However, the relative influence of these indices differs. To evaluate the forming quality, the ideal point method of multi-objective programming was used to establish the optimization function, taking the three forming indices as variables. It was necessary to normalize  $I_w$ ,  $I_f$ , and  $I_t$  to balance the effect of each index on the forming quality. The smaller the forming indices are, the better the forming quality is; therefore, the ideal point was defined as the point where the three forming indices are zero. The distance between the normalized forming result and the ideal point was defined as the optimization function. The optimization function and boundary conditions are shown in Equations (4) and (5):

$$\min I = [(I_w/I_{w0})^2 + (I_f/I_{f0})^2 + (I_t/I_{t0})^2]^{\frac{1}{2}} \tag{4}$$

$$s.t. \begin{cases} 0 < I_w \leq I_{w0} \\ 0 < I_f \leq I_{f0} \\ 0 < I_t \leq I_{t0} \end{cases} \tag{5}$$

where  $I$  is the target value of forming quality, and the smaller  $I$  is, the better the forming quality is.  $I_{w0}$ ,  $I_{f0}$ , and  $I_{t0}$  are the maximum allowable values of corresponding forming indices, which are 2%, 10% and 25%, respectively.

The hollow section parameters were optimized based on the grey wolf optimizer, which was first proposed by Mirjalili [20]. This algorithm is an optimization method inspired by the prey hunting activities of grey wolves. Thanks to the characteristics of strong convergence, fewer parameters, and easy programming, it has been widely used in various fields in recent years.

Figure 13 shows the procedure of the optimization algorithm. First, the grey wolf population was initialized and a set of random numbers was taken as the first set of parameters of the hollow mandrel. As the numerical results in Tables 6 and 7 are discrete, forming results were obtained by bilinear interpolation method. The hollow mandrel parameters were then updated by comparing the value of the fitness function, and a new

set of hollow mandrel parameters was generated. This process was repeated until the maximum number of iterations was reached.

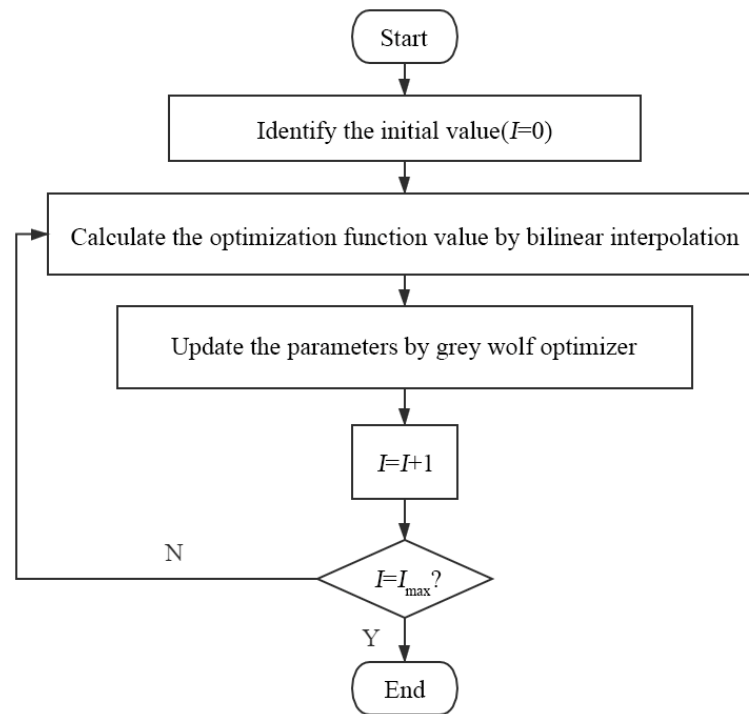


**Figure 13.** Flowchart of the optimization progress.

The maximum number of iterations was 1000. To display the convergence of the algorithm, the curve of the optimization function value with the top 50 iterations is shown in Figure 14.

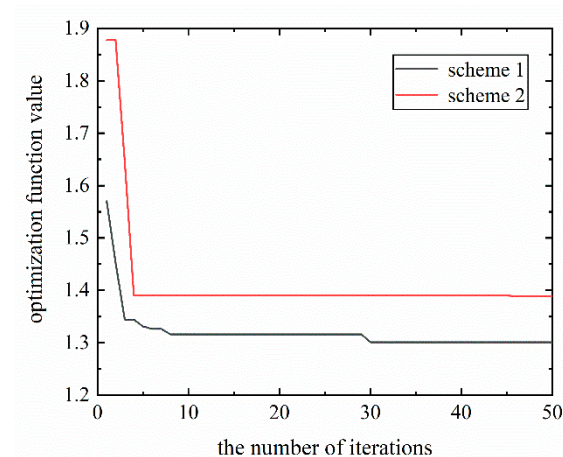


**Figure 14.** Convergence curve.

The optimal hollow section parameters and corresponding forming results of the two schemes are shown in Table 8. Among the three forming indices,  $I_w$  was the most optimized. Compared with the ordinary non-ball mandrel,  $I_w$  was decreased by 45.90%,  $I_f$  was decreased by 9.28%, and  $I_t$  was decreased by 3.41% in scheme 1. In scheme 2,  $I_w$ ,  $I_f$ , and  $I_t$  were reduced by 38.52%, 7.61%, and 3.97% compared with the solid mandrel, respectively. The forming indices meet the quality requirements and the forming quality was improved when using hollow mandrels. Considering the convenience of processing

and the small difference in forming quality, the hollow mandrel with a regular cylindrical hollow section (scheme 2) is recommended, even though the forming quality of scheme 1 was slightly better.

**Table 8.** Optimal parameters of the hollow section and corresponding forming results.

Mandrel Shape	$L/\text{mm}$	$t/\text{mm}$	$I_w/\%$	$I_f/\%$	$I_t/\%$	$I$
Solid mandrel	-	-	2.44	8.94	19.92	1.7095
Hollow mandrel scheme 1	120	11	1.32	8.11	19.24	1.2983
Hollow mandrel scheme 2	120	13	1.50	8.26	19.13	1.3529

#### 4. Conclusions

To explore the feasibility of a non-ball mandrel in thin-walled tube cold bending, we proposed two hollow mandrel schemes. Based on numerical calculations, we reached the following conclusions:

1. Small radius cold bending of thin-walled tubes using an ordinary non-ball mandrel does not meet the forming requirements. Therefore, two kinds of hollow non-ball mandrel schemes were proposed to obtain satisfactory forming results;
2. Comparing the two hollow mandrel schemes, the influence of tested parameters on the forming indices were similar. The hollow section thickness had the greatest influence of the parameters measured. In scheme 1, as the hollow section thickness increased from 6 to 11 mm, the wrinkling rate declined by 45.58%. When the thickness increased from 11 to 15 mm, the wrinkling rate increased by 78.21%. In scheme 2, the wrinkling rate first decreased by 39.41% and then increased by 51.44% as the thickness increased. The wrinkling rate was lowest when the hollow section thickness was 11 mm in scheme 1 and 13 mm in scheme 2. As the hollow section thickness increased, the flattening rate decreased by 60.49% and 63.83% in scheme 1 and scheme 2, respectively. As the hollow section thickness increased, the thinning rate increased by 35.44% and 41.02% in scheme 1 and scheme 2, respectively.
3. Improved hollow section parameters were obtained based on the ideal point method and grey wolf optimizer. It was shown that it is feasible to use a hollow non-ball mandrel instead of a ball mandrel for cold bending of thin-walled tube with a small radius;
4. Both the hollow mandrel scheme with a cylinder-like hollow section and a regular cylindrical hollow section met the forming requirements for a tube. Considering that the mandrel with a regular cylinder hollow section has the advantages of simple processing and its forming quality is similar to that of the cylinder-like hollow section, we recommend this design for use.

**Author Contributions:** Conceptualization, L.B. and J.L.; methodology, L.B. and J.L.; software, Z.W.; validation, Z.W. and S.Z.; formal analysis, L.B.; investigation, L.B. and J.L.; resources, J.L.; data curation, L.B.; writing—original draft preparation, L.B.; writing—review and editing, J.L.; visualization, L.B.; supervision, J.L.; project administration, J.L. All authors have read and agreed to the published version of the manuscript.

**Funding:** This research received no external funding.

**Institutional Review Board Statement:** Not applicable.

**Informed Consent Statement:** Not applicable.

**Data Availability Statement:** All data are included in the paper.

**Conflicts of Interest:** The authors declare no conflict of interest.

## References

1. Yang, H.; Sun, Z.C.; Lin, Y. Advanced plastic processing technology and research progress on tube forming. *J. Plast. Eng.* **2001**, *8*, 83–85.
2. Liu, Z.W.; Dong, F.F.; Li, L.X.; Yao, Z.Q. Process Parameters Optimization of Rotary Draw Bending for Large Diameter Thin-walled Steel Tube for Automotive Bumper. *Automot. Eng.* **2015**, *37*, 853–860.
3. Shen, S.J.; Yang, H.; Li, H.; Zhan, M. Experimental study on role of mandrel in thin walled tube NC bending process with small bending radius. *J. Plast. Eng.* **2007**, *14*, 29–34.
4. Nakajima, K.; Utsumi, N.; Saito, Y.; Yoshida, M. Deformation property and suppression of ultra-thin-walled rectangular tube in rotary draw bending. *Metals* **2020**, *10*, 1074. [[CrossRef](#)]
5. Utsumi, N.; Sakaki, S. Countermeasures against undesirable phenomena in the draw-bending process for extruded square tubes. *J. Mater. Process. Technol.* **2002**, *123*, 264–269. [[CrossRef](#)]
6. Różyło, P. Optimization of I-section profile design by the finite element method. *Adv. Sci. Technol. Res. J.* **2016**, *10*, 52–56. [[CrossRef](#)]
7. Tsumura, K. Hierarchically aggregated optimization algorithm for heterogeneously dispersed utility functions. *IFAC Pap. Online* **2017**, *50*, 14442–14446. [[CrossRef](#)]
8. Chen, J.Y.; Sun, Y.J. A new multiplexed optimization with enhanced performance for complex air conditioning systems. *Energy Build.* **2017**, *156*, 85–95. [[CrossRef](#)]
9. Farzampour, A.; Khatibinia, M.; Mansouri, I. Shape optimization of butterfly-shaped shear links using grey wolf algorithm. *Ing. Sismica* **2019**, *36*, 27–41.
10. Li, H.; Yang, H.; Zhan, M.; Sun, Z.C.; Gu, R.J. Role of mandrel in NC precision bending process of thin-walled tube. *Int. J. Mach. Tools Manuf.* **2007**, *47*, 1164–1175.
11. Li, H.; Yang, H.; Zhang, Z.Y.; Li, G.J.; Liu, N.; Welo, T. Multiple instability-constrained tube bending limits. *J. Mater. Process. Technol.* **2014**, *214*, 445–455. [[CrossRef](#)]
12. Li, H.; Yang, H.; Zhang, Z.; Wang, Z. ‘Size effect’ related bending formability of thin-walled aluminum alloy tube. *Chin. J. Aeronaut.* **2013**, *26*, 230–241.
13. Zhao, Y.; Liu, J.; Tang, W.Y.; Zou, S.G. Rapid prediction of small radius bending forming results based on MPSO-BP model. *J. Plast. Eng.* **2018**, *25*, 122–128.
14. Wang, Z.A.; Liu, J. Shape parameter optimization of mandrel for tube bending based on orthogonal experimental design. *J. Plast. Eng.* **2020**, *27*, 59–65.
15. Dang, C.K. Selection of mandrel for steel tube cold bending forming. In Proceedings of the Annual Meeting of the Society of Mechanical Engineering, Henan, China, 1 September 2002; pp. 116–119.
16. Wu, C.; Yan, Y.; Hu, Z.L. Effect of mandrel on the forming quality of thin walled tube. *Hydro Mechatron. Eng.* **2015**, *43*, 52–59.
17. Zheng, C.Y.; Liu, D.X.; Liu, Y.; Li, Y.M.; Tian, X. Analysis on the effects of material models on wall thickness variation of tube bending based on numerical simulation. *J. Plast. Eng.* **2010**, *17*, 23–26.
18. Wen, X. Study of Small Radius Tube Bending with Numerical Experiment Based on Response Surface Methodology. Master’s Thesis, Shanghai Jiao Tong University, Shanghai, China, 2015.
19. Zhuang, Z.; You, X.C. *Finite Element Analysis and Application based on ABAQUS*, 1st ed.; Tsinghua University Press: Beijing, China, 2009; p. 111.
20. Mirjalili, S.; Mirjalili, S.M.; Lewis, A. Grey wolf optimizer. *Adv. Eng. Softw.* **2014**, *69*, 46–61. [[CrossRef](#)]